



Ministry of Science, Research & Technology
Iranian Research Organization
for Science and Technology

Research paper

Combustion synthesis of sponge-like CeO₂ powder for selective determination of uric acid in biological fluids

Zahra Hashemzaei¹, Hamideh Saravani^{1,*}, Mahmood Sharifitabar^{2,*}, Mehdi Shahbakhsh³

¹ Inorganic Research Laboratory, Department of Chemistry, University of Sistan and Baluchestan, Zahedan, Iran

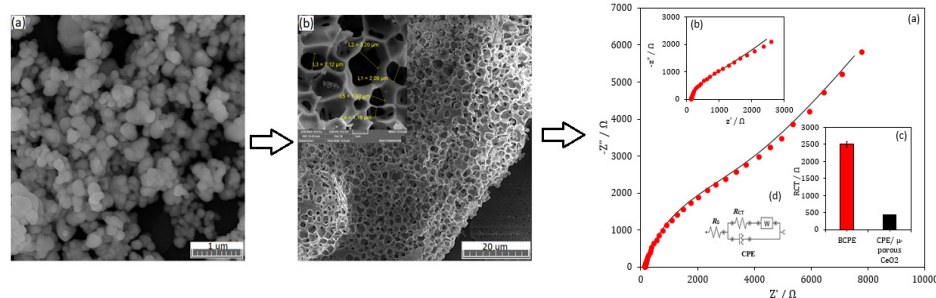
² Department of Materials Engineering, Faculty of Engineering, University of Sistan and Baluchestan, Zahedan, Iran

³ Analytical Research Laboratory, Department of Chemistry, University of Sistan and Baluchestan, Zahedan, Iran

HIGHLIGHTS

- Synthesis of porous Mg-doped CeO₂ powder by the combustion synthesis route.
- Application of synthesized porous CeO₂ powder for selective determination of uric acid.
- Obtaining excellent results for ultra-trace voltammetric determination of UA.

GRAPHICAL ABSTRACT



ARTICLE INFO

Article history:

Received 9 April 2022

Revised 28 May 2022

Accepted 2 June 2022

Keywords:

Porous cerium oxide
Modified carbon paste electrode
Uric acid
Voltammetric determination

ABSTRACT

Sponge-like porous cerium oxide particles were prepared through the self-propagating high-temperature synthesis process. Then, the synthesized powder was used to modify the carbon paste electrode (CPE/porous CeO₂) for voltammetric determination of uric acid (UA) in biological fluids. Under optimal conditions, the linear concentration-response relationship was in the range of 0.25-10 and 10-300 μM, and a detection limit of 60 nM (S/N=3) was obtained. In addition, the proposed sensor showed excellent selectivity towards UA over common co-existing species such as ascorbic acid, ibuprofen, dopamine, and acetaminophen. Good repeatability of sensor responses (Relative standard deviation (RSD) < 3.2%), superior reproducibility (RSD < 2.8%), and excellent storage stability (error < 5% after 1 month storage at room temperature) along with appropriate recovery values (in the range of 99.2 -102.7%) demonstrate the applicability of CPE/porous CeO₂ for the determination of UA levels in biological fluids.

1. Introduction

Uric acid (UA), chemically designated as 2,6,8-trihydroxypurine as a purine degradation product, is an antioxidant that exists in biological fluids like urine and blood serum. People with diseases such as gout, xanthinuria, toxemia during pregnancy, leukemia, and renal failure have abnormal levels of UA in their bodies [1]. The normal concentration levels of UA in humans are 130-460 μM in serum and 1.49-4.46 mM in urine [2].

Detection of UA (Fig. 1) is of great significance in physiological and pathological diagnosis because of its electrochemically active nature. UA is generally determined by electrochemical methods, but various methods such as chemiluminescence [3], high-performance liquid chromatography [4], and ultraviolet-visible spectroscopy have been reported for selective detection of UA. However, the above methods are generally costly and time-consuming [5]. Hence, electrochemical techniques have attracted a great deal of interest due to their simplicity, low cost, good sensitivity, high selectivity, and how rapid the detection can be carried out [6]. Unfortunately, UA determination using a bare graphite paste electrode (BCPE) shows high over-potential, irreversibility, and fouling effects. Enzymatic sensors based on uricase are commonly utilized for the selective determination of uric acid, but they also suffer from non-idealities such as high cost, the need for enzyme immobilization at the surface of an electrode, and control of operational conditions such as pH and temperature [7]. Therefore, chemically modifying electrodes (CME) with nano-materials and porous materials with high surface areas can help in overcoming these deficiencies. Different materials like metal oxide, fullerene, carbon nanotubes, polymers, nanocomposites, and graphene have been used as modifiers in the past decades. In recent years, uric acid has attracted the widespread attention of many researchers. For example, Chunran Ma *et al.* investigated a novel ratiometric fluorescence

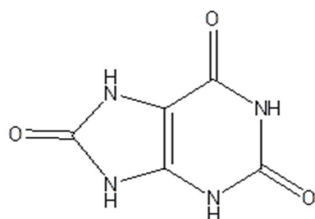


Fig. 1. The chemical structure of uric acid (UA).

nanoprobe based on CD@ZIF-CuNC nanocomposites [8], Xiu Qin *et al.* studied enzyme-free colorimetric based on inhibition of gold nanorods [9], and Dan Cao *et al.* reported enzyme-free fluorescence in serum using Si/N doped carbon dots [10].

Semiconductor materials like cerium (IV) oxide are used in various applications such as electronics, super capacitors, sensors, fuel cells, photo electronics, solar cells, and electro catalysis [11,12]. Rapid transition of the oxidation state of cerium between $\text{Ce}^{(\text{III})}$ and $\text{Ce}^{(\text{IV})}$ leads to its interesting electro catalytic activity [13]. This property depends on the oxygen vacancy concentration in the structure of CeO_2 , which may be controlled by doping [13,14]. Various elements can be doped in CeO_2 using methods such as microwaves [15], sol-gel [16], hydrothermal [17], solvothermal [14], and solution combustion processes [18]. Alternatively, the concentration of vacancy in the crystalline structures can be increased by rapid cooling from high temperatures [19]. Therefore, the catalytic activity of CeO_2 may be improved by rapidly cooling heated elements. In addition, the formation of a porous microstructure will increase the contact surface between the catalysis and the electrolyte.

Self-propagating high-temperature synthesis is a fast, facile, easy-echo, and promising route to obtain different types of materials, including oxides, borides, carbides, etc. During this process, the raw materials of an exothermic reaction are mixed and pressed into a compact. Then, the reaction is initiated locally. The liberated heat will result in self-sustaining propagation of the reaction along the compact [20].

In a previous study, the authors synthesized Mg-doped porous CeO_2 through a novel combustion synthesis route [18]. Other researchers have reported the application of CeO_2 for the electrochemical determination of many biomolecules, including ascorbic acid (AA), urea, and dopamine [21]. Accordingly, in this study, a novel electrochemical sensor based on the combustion synthesized porous CeO_2 modified graphite paste electrode (CPE/porous CeO_2) was prepared and subsequently used to determine UA in biological fluids.

2. Experimental procedure

2.1. Materials

Mg powders (purity 99%), CeO_2 (purity 99.9%), sodium hydroxide (purity 99.8%), phosphoric acid

(99.6%), graphite powder (as conductive material), and paraffin oil (DC 350, density = 0.88 g.cm⁻³ as binding agents) were purchased from the Merck Company. In addition, oxygen gas with purity > 99% was used. UA was obtained from Sigma-Aldrich, and urine and blood samples were taken from the Mehran Clinical Laboratory (Zahedan, Iran) without any sample pretreatment.

2.2. Methods

2.2.1. Synthesis of porous CeO₂

Porous CeO₂ was obtained by the self-propagating high-temperature synthesis method [22]. Briefly, a mixture containing 0.05 mol CeO₂ and 1 mol Mg powders was prepared by hand-mixing for 20 min. Then, the powder mixture was pressed in a cylindrical steel die (12 mm diameter) using 160 MPa compaction pressure. Next, the self-propagating high-temperature reaction was initiated by passing a direct electrical current (150 A) through a 1.6 mm diameter tungsten electrode located at the top of the compact. Once initiated, a wave of exothermic reaction propagated in the remaining reactants. Reactions have been completed in a closed chamber containing 99% pure oxygen gas at a pressure slightly higher than 1 atm as follows:



After the reaction was terminated, the combustion products were leached out with a 6 M HCl solution to remove the unwanted MgO phase. Finally, the product was washed several times with distilled water and dried at 100 °C for 1 h in an electric oven. The final product was denoted as porous CeO₂.

2.2.2. Fabrication of the CPE/porous CeO₂ sensor

First, 5 mg of porous CeO₂ and 195 mg graphite were mixed. Next, a few droplets of paraffin oil were added (5 mg). The mixing operation was conducted by a mortar and pestle for 10-15 min. Then, the prepared carbon paste was well packed into a glass tube with an internal diameter of 0.24 cm. Finally, electrical contact was made by inserting a copper wire into the paste. The new surface was obtained by pushing the graphite paste out of the glass tube and polishing it on weighing paper.

2.2.3. Characterization of the CPE/porous CeO₂ sensor

All measurements were performed by an electroanalyzer system (SAMA 500, I.R. Iran) coupled with a personal computer. The electrochemical measurements were carried by a typical three-electrode cell at 25 ± 1 °C. A saturated silver/silver chloride electrode (Ag/AgCl) and a platinum electrode (Pt) were employed as the reference and counterparts, respectively. A field emission scanning electron microscope (FESEM MIRA3 TESCAN) and energy dispersive X-ray analysis (EDX SAMX) were employed for microstructural and chemical analyses, respectively. Electrochemical impedance spectroscopy (EIS) was performed via a potentiostat/galvanostat (Autolab PGSTAT 128N, EcoChemie, Netherlands) controlled with NOVA 1.11 software. Electrochemical impedance spectroscopy was carried out in 5 mM [Fe(CN)₆]^{3-/4-} as a redox probe and performed in 0.1 M KCl. A pH meter (Model 744, Metrohm) was used for pH measurements.

3. Results and discussion

3.1. Characterization of porous CeO₂

The FE-SEM micrograph of the primary CeO₂ with spherical morphology is shown in Fig. 2(a). The mean particle size of cerium oxide measured by the dynamic light scattering method was 1.5 μm. Fig. 2(b) shows that the melting of CeO₂ and MgO, the distribution of the melts between each other at high temperatures, and the subsequent removal of MgO from the combustion products by acid leaching leads to the formation of porous CeO₂. The volume percent of pores calculated by image processing software was 50%. In addition, the pore sizes mostly varied between 1 to 5 μm. The BET surface area of the primary powder was measured as 2.8 m².g⁻¹ but decreased to 0.5 m².g⁻¹ in the porous CeO₂ after combustion synthesis and the subsequent leaching process [18]. Although the formation of the melted structure slightly reduced the surface area of the primary powders, it is expected that the continuous network of porous CeO₂ can facilitate the electron transfer rate in this compound.

The EDS map distribution of elements in the porous microstructure is shown in Fig. 3 (a)-(d). The uniform distribution of Ce and O certified the formation of CeO₂ structure (Figs. 3(b) and 3(c)). In addition, the presence

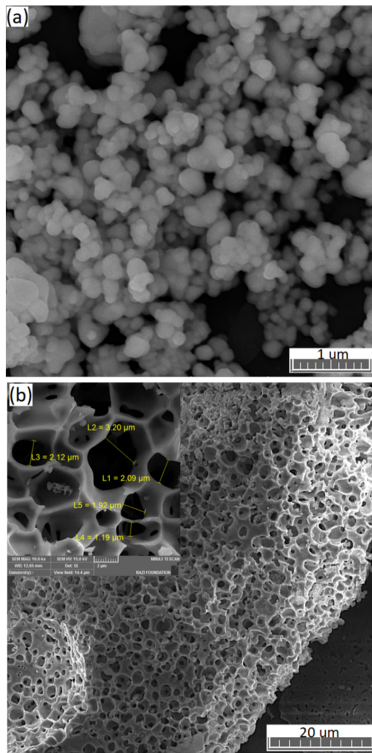


Fig. 2. FE-SEM micrographs of the (a) primary CeO_2 and (b) Porous CeO_2 obtained by the combustion synthesis route.

of Mg in the structure of CeO_2 showed that this element doped into the structure of CeO_2 at high temperatures (Fig. 3 (d)). The doping of Mg in the structure of CeO_2 was proven in our previous study [18]. Therefore, it is concluded that a porous Mg-doped CeO_2 powder was tuned through the combustion synthesis route.

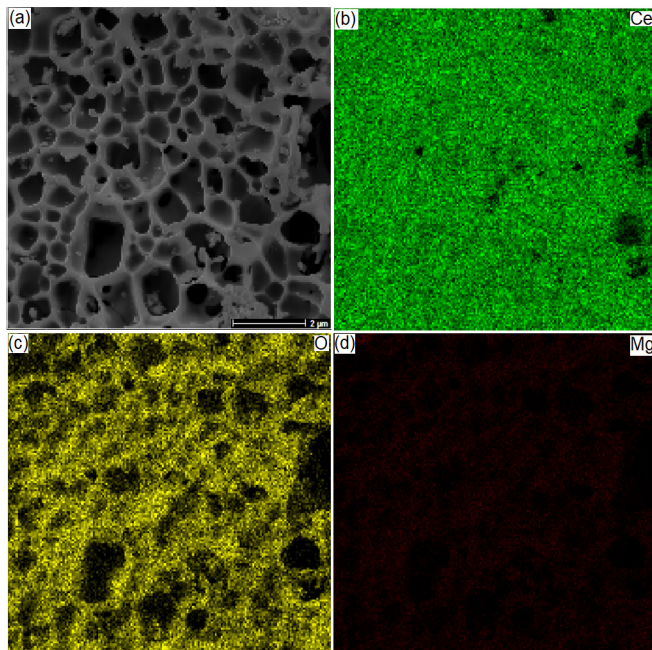


Fig. 3. The EDS elemental map analysis of the synthesized porous CeO_2 . (a) FE-SEM image, (b) mapping image of Ce elements, (c) mapping image of O elements, (d) mapping image of Mg elements.

Cyclic voltammetry is a powerful technique for investigating electrochemical behaviors of modifiers and electroactive analytes on the surface of electrodes. Therefore, the presence of electroactive species on the surface of CPE/porous CeO_2 was further confirmed using cyclic voltammetry analysis. Fig. 4(a) shows cyclic voltammograms of CPE/porous CeO_2 in 0.1 M PBS (pH = 3) that are attributed to the redox peaks of metal oxide ($\text{Ce}^{3+}/\text{Ce}^{4+}$) at 0.241 and 0.213 V [23]. The stepwise modification of BCPE was monitored by CV and EIS containing a solution of 5 mM $\text{Fe}(\text{CN})_6^{3-/4-}$ in a 0.1 M KCl solution. The CV graph of the bare CPE (BCPE) shows redox peaks at 0.43 and -0.04 V with peak currents of 245 and 236 μA , as seen in Fig. 4(b). On the other hand, the CV graph of CPE/porous CeO_2 shows redox peaks at 0.32 and 0.09 V with peak currents of 400 and 397 μA , respectively. Compared to BCPE, the increase in peak currents and decrease in peak potentials for CPE/porous CeO_2 are due to the electro-catalytic activity of porous CeO_2 .

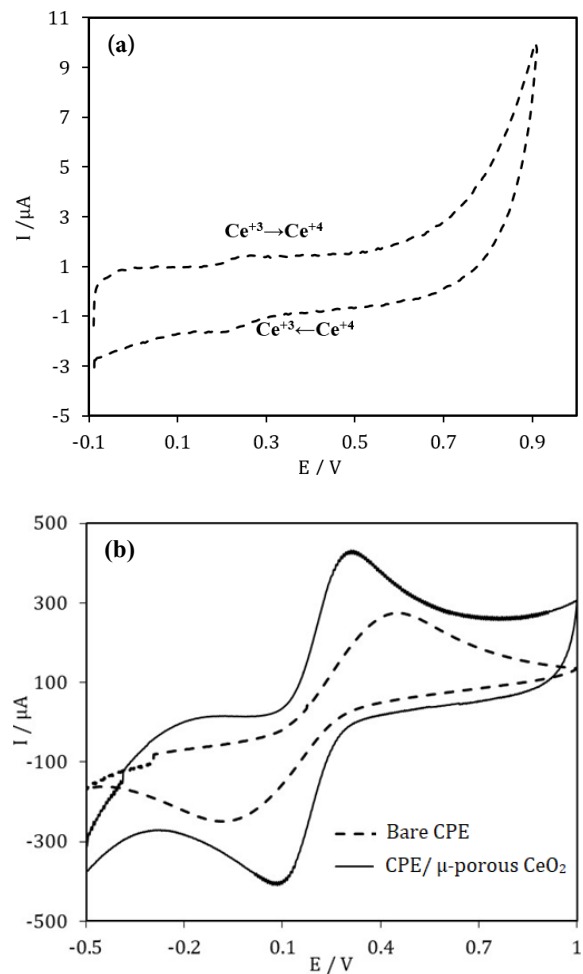


Fig. 4. (a) the CVs graph of CPE/porous CeO_2 in 0.1M PBS (pH = 3) and (b) the CVs graph of 0.1 M KCl containing 5 mM $\text{Fe}(\text{CN})_6^{3-/4-}$ for BCPE and CPE/porous CeO_2 with Scan rate of 100 $\text{mV}\cdot\text{s}^{-1}$.

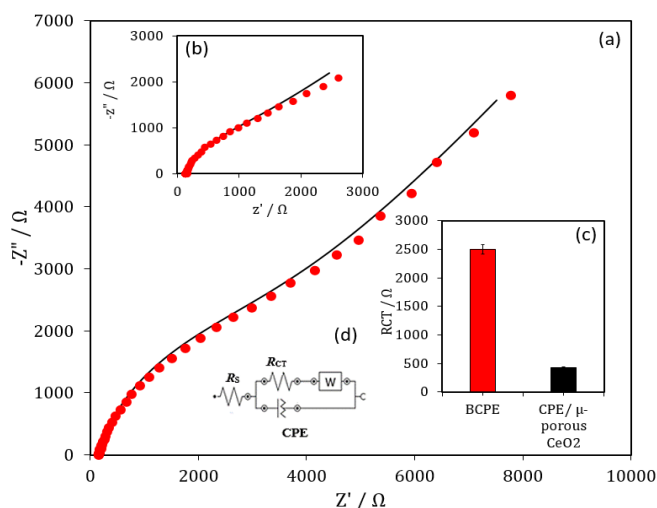


Fig. 5. (a) Nyquist plot of BCPE in 0.1M KCl containing 5 mM Fe(CN)₆^{3-/4-}, (b) Nyquist plot of CPE/porous CeO₂ in 0.1 M KCl containing 5 mM Fe(CN)₆^{3-/4-}, (c) R_{ct} values for BCPE and CPE/porous CeO₂ (the error bars represent the standard deviation of three parallel tests), (d) Equivalent circuit.

R_s : solution resistance, R_{ct} : charge transfer resistance, W : Warburg element. CPE: Constant Phase Element. EIS was performed on a range of frequencies from 10 kHz to 0.1 Hz at an amplitude of 10 mV, and it was superimposed on the formal potential of the redox probe ($E^{0'} = E_{1/2} = (E_{pa} + E_{pc})/2$, when $D_{ox} = D_{red}$), which was calculated from cyclic voltammograms.

Fig. 5 shows the Nyquist plot of BCPE and CPE/porous CeO₂. Fitting and simulation of electrochemical impedance spectroscopy (EIS) data were done using NOVA software. Randle's equivalent circuit, shown in Fig. 5(c), was selected as an equivalent circuit for fitting/simulation of EIS data. The R_{ct} (\pm RSD) for CPE/porous CeO₂ and BCPE were 430 (\pm 2.8) and 2500 (\pm 3.5) Ω , respectively. The considerable decrease in R_{ct} of CPE/porous CeO₂ compared to BCPE is attributed to the higher electrical conductivity and continuous network of porous CeO₂. Moreover, the lower R_{ct} value for CPE/porous CeO₂ compared to BCPE indicates the facility of the electron transfer kinetics.

3.2. Electrochemical characterization of BCPE and CPE/porous CeO₂ for determination of UA

Cyclic voltammetry was used to compare the electrodes' responses toward UA. Fig. 6 shows the CVs of BCPE and CPE/porous CeO₂. The BCPE shows broad and weak oxidation peaks for UA at 0.60 V. While the electrochemical performance of a bare CPE (BCPE) is not suitable for the stable determination of UA, the CPE/porous CeO₂ shows a strong oxidation peak for UA at 0.57 V. As shown in this figure, the CVs of the

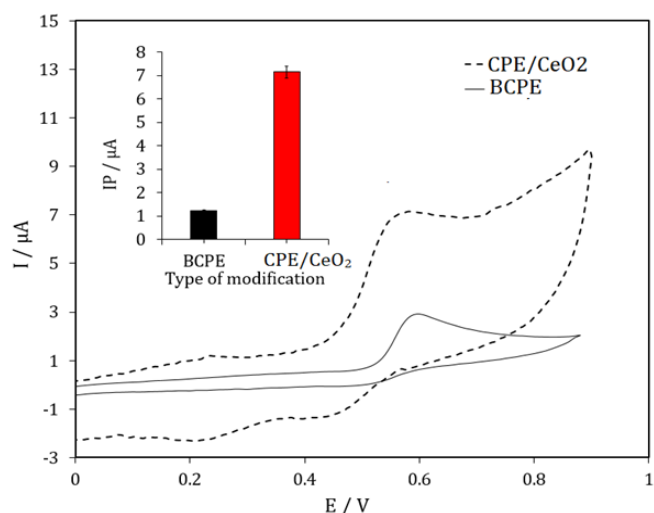


Fig. 6. The CVs graphs of BCPE and CPE/porous CeO₂ in 0.1M PBS (pH = 3) containing UA (100 μ M). Inset shows peak currents for BCPE and CPE/porous CeO₂.

oxidation peak potential of UA at the CPE/porous CeO₂ shifted in the positive direction compared to BCPE. The results show the electro-catalytic activity for the CPE/porous CeO₂. Therefore, this electrode can be used for sensitive determination of UA. This excellent electro-catalytic activity is attributed to the presence of cerium ions with inter-convertible oxidation states, good electrical conductivity, and the high surface area of porous CeO₂ [14].

3.3. The effect of scan rates

Cyclic voltammetry was performed at various scan rates to determine if the electrochemical reaction of

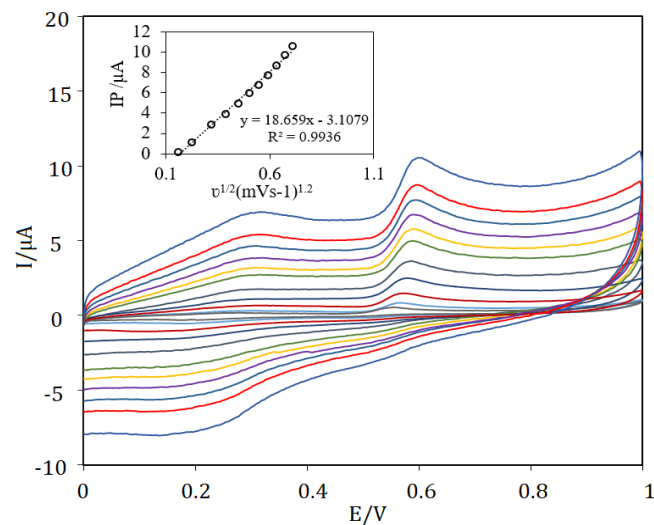


Fig. 7. The CVs graph of CPE/porous CeO₂ in 0.1 PBS (pH = 3) containing UA (10 μ M at various scan rates (25 to 500 $mV \cdot s^{-1}$). Inset shows plots of anodic peak currents vs. square root of scan rate.

uric acid at the CPE/porous CeO₂ is diffusion-controlled or surface-confined. In the former, the peak currents are directly proportional to the square root of the scan rate, and in the latter, the peak currents are directly proportional to the scan rate [24]. As shown in Fig. 7, for the UA peak, the currents are proportional to the square root of the scan rate, and the plot of peak currents (I_p) vs. the square root of scan rate ($v^{1/2}$) is linear in the range of 25 to 500 mV.s⁻¹, indicating diffusion-controlled processes for UA at sufficient over-potentials.

3.4. Repeatability, reproducibility, and storage stability

The relative standard deviation (%RSD) for ten replicate measurements of 0.5 and 50 μM UA were 2.4% and 2.8%, respectively, indicating good repeatability of the analytical signals of the CPE/porous CeO₂. In addition, Fig. 8 shows that the %RSD of all UA concentrations is lower than 4% ($n=3$).

Furthermore, to prove the reproducibility of the electrode preparation, five different modified electrodes were prepared and applied to measure two different concentrations of UA. The values of %RSD were 2.8% for 0.5 μM and 3.2% for 25 μM, which proves the excellent reproducibility of signals of CPE/porous CeO₂ toward UA. Furthermore, as shown in Fig. 8, the storage stability of the modified electrode was examined by analyzing a solution containing 140 μM in 0.1 M PBS after 0, 15, and 30 days. The results show that the response decreased to 97.0 and 95.5% of its initial

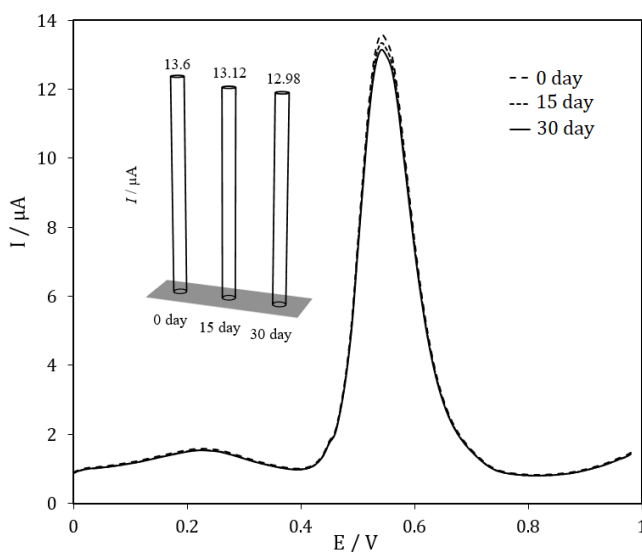


Fig. 8. The differential-pulse voltammetry (DPV) graphs of CPE/porous CeO₂ in 0.1M PBS (pH = 3) containing UA (140 μM) after 0, 15 and 30 storage days.

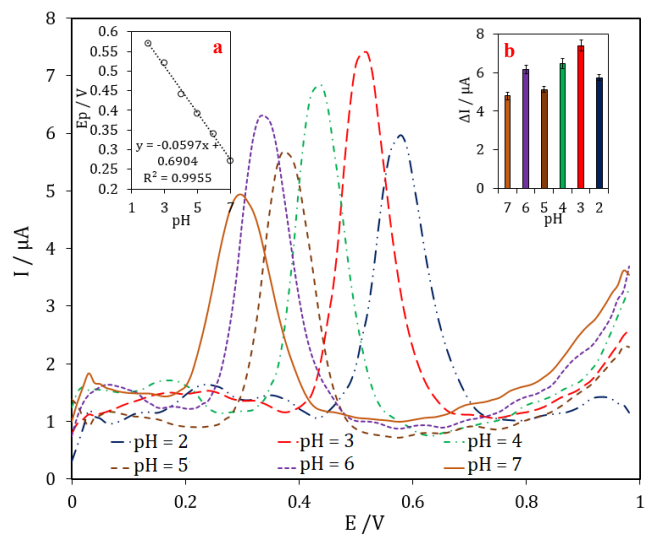


Fig. 9. The differential-pulse voltammetry (DPV) graphs of a solution containing UA (60 μM at CPE/porous CeO₂ in 0.1M PBS) at various pH values (2-7). Inset (a) plots of peak potentials versus pH. Inset (b) peak currents versus pH.

value after 15 and 30 days, respectively. Therefore, the CPE/porous CeO₂ presents excellent storage stability, superior reproducibility, and good repeatability, indicating its promising utility for precise analysis of UA.

3.5. pH effect

pH is an important parameter in the electro-oxidation of bio-molecules as well as the electro-catalytic activity of electro-catalysts. Therefore, the effect of pH on the electro-chemical response of CPE/porous CeO₂ to UA was investigated. The effect of pH on the CPE/CeO₂ electro-chemical response in 0.1 M PBS containing UA (70 μM) at various pH values is shown in Fig. 9.

Contributing protons in the electro-chemical reaction causes the peak potential for UA to shift to negative potentials via an increase in solution pH. Moreover, Fig. 9 shows that UA's highest peak currents were obtained at pH = 3. The linear relationship between the peak current and pH is illustrated in the Fig. 9 inset. The linear regression equations (Eq. (1)) is as follows;

$$E_{(pa,UA)}(\text{V}) = 0.6904 (\pm 0.01) - 0.0597 (\pm 0.002) \text{pH} \quad (r^2 = 0.9955) \quad (1)$$

where, the slopes of the regression equations are close to the theoretical value of 0.0585 V/pH for a process that involves two electrons and two protons [24,25]. The likely electrochemical reaction of UA at the

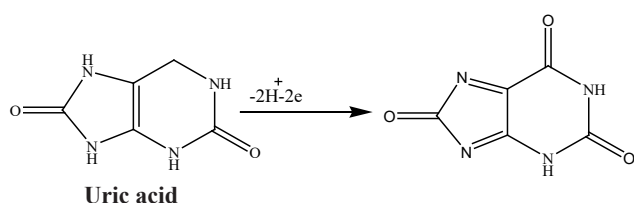


Fig. 10. The electrochemical reaction of UA at the surface of the CcO_2 electrode.

surface of the CPE/porous CcO_2 electrode should be a two-electron and two-proton process (Fig. 10) [26]. Eventually, pH 3.0 PBS was selected as the optimum pH for electro-catalysis of UA oxidation on the surface of the CPE/porous CcO_2 electrode.

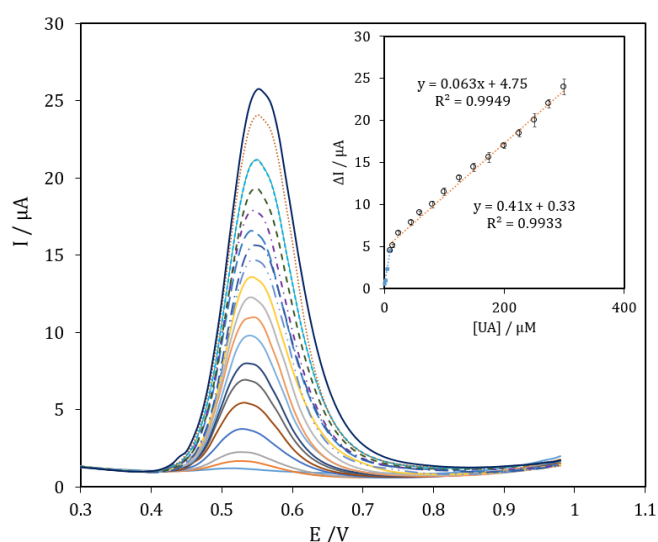


Fig. 11. The DPVs graphs of CPE/porous CcO_2 in 0.1 M PBS (pH = 3) containing increasing concentrations of UA. [UA]:0.25 - 300 μ M. The inset shows the plot of anodic peak currents vs. concentration of UA. The error bars represent the standard deviation of three parallel tests (relative standard deviation (%RSD) was found to be < 4% for $n = 3$).

3.6. Voltammetric determination of UA

DPV is a more sensitive technique than CV because of the minimal contribution of the capacitive current. Therefore, voltammetric determination of UA was carried out using the DPV technique. Fig. 11 shows the calibration curves obtained by measuring the DPV peak currents for increasing concentrations of UA at the surface of CPE/porous CcO_2 .

The observed linear concentration–response relationship was based on the linear relationships of $\Delta I = 0.41 (\pm 0.01) [UA (\mu M)] + 0.33 (\pm 0.11)$, ($R^2 = 0.9976$) and $\Delta I = 0.063 (\pm 0.002) ([UA (\mu M)] + 4.75 (\pm 0.26))$, and ($R^2 = 0.9949$) in the concentration ranges of 0.25 - 10

Table 1. Interference effect of foreign species in the electrochemical determination of UA (10 μ M).

Foreign species	5% tolerable molar ratio*
Mg^{2+} , Cr^{3+} , Na^+ , K^+ , Ca^{2+} , NO_3^- , Cl^- , PO_4^{3-} , SO_4^{2-}	>500
Glucose, NO_2^-	>100
Ascorbic Acid, dopamine	>15
Ibuprofen	>12
Acetaminophen	>10

*In a certain range of concentrations, an analyte has no interference if it causes a relative error less than or equal to ± 5 (%).

and 10 - 300 μ M, respectively. The smaller slope in the second linear segment is likely due to kinetic limitations [27]. The detection limit was calculated as 60 nM based on the relationship limit of detection ($LOD = 3S_{blank}/m$), in which S_{blank} demonstrates the standard deviation of blank signals ($n = 10$) and m is the slope of the calibration curve. Moreover, to investigate the selectivity of the CPE/porous CcO_2 for UA, its electrochemical response toward UA in the presence of other coexisting species like ascorbic acid, ibuprofen, acetaminophen, and other interfering species was investigated. Results revealed that these species show no interfering effect in the voltammetric determination of UA. The outcomes are illustrated in Table 1.

In addition, the electro-chemical response of CPE/porous CcO_2 toward UA was compared with recently published works [28-35]. As depicted in Table 2, in most cases, the proposed sensor shows a lower detection limit and broader linear concentration range, or in other cases, it shows comparable ones. It is worth mentioning that the proposed sensor was prepared by a simple, inexpensive, and fast method compared to other sensors that use expensive polymers, composites, and nanomaterials. Therefore, our sensor can be introduced as a promising alternative for determining UA. Like many solid electrodes, electrode fouling was a problem due to the accumulation of UA oxidation products. The advantage of the graphite paste electrode is when necessary, the electrode surface can be regenerated by pushing the graphite paste out of the glass tube and polishing it with weighing paper.

3.7. Analysis of real samples

To examine CPE/porous CcO_2 for actual samples, its DPVs were taken in human urine and serum samples.

Table 2. Comparison of the proposed method with other electroanalytical methods for the simultaneous determination of UA.

Electrode	Modifier	Method	pH	Analyte	Linear range (μM)	Detection Limit (μM)	Ref.
GCE	^a MWCNT@FC-2	DPV	6	UA	0.5-500	0.3	[28]
GCE	^b PEDOT-GO	DPV	7.4	UA	40-240	10	[29]
GCE	^c PEDOT/PANI	DPV	7	UA	3-100	0.41	[30]
CPE	^d CuO-rGR/1M3OIDTFB/CPE	SWV	7.4	UA	0.4-400	0.08	[36]
GCE	ZrO ₂ /ZnO NPs	DPV	7	UA	10-2400	0.29	[32]
GCE	^e HMT-PMBI	DPV	7	UA	5-200	7.7	[33]
GCE	rGO/CS/Cr ₂ O ₃	DPV	7	UA	10-500	0.8	[34]
GCE	Ni-ZIF-8/N S-CNTs/ CS	DPV	5.5	UA	1-600	0.41	[35]
CPE	Porous CeO₂	DPV	3	UA	0.25-10, 10-300	0.06	Present work

(a) multi-walled carbon nanotubes ferric ceria nanofibers (MWCNT@FC-2)

(b) Poly(3,4-ethylenedioxythiophene) graphene oxide (PEDOT-GO)

(c) poly(3,4-ethylenedioxythiophene) (PEDOT) / polyaniline (PANI)

(d) copper oxide decorated reduced graphene/1-methyl-3-octylimidazolium tetrafluoroborate (CuO-rGR/1M3OIDTFB/CPE)

(e) hexamethyl-pterphenyl poly (benzimidazolium) (HMI-PMBI).

For this purpose, urine and serum samples were diluted 200 and 60 fold with PBS (0.1M, pH = 3) without further pretreatment. As can be seen in Table 3, the concentration of UA in real samples was determined using the standard addition method. Moreover, a relative standard deviation (RSD) of less than 5% and appropriate recovery values (in the range of 99.2 -102.7) for spiked samples indicate that the modified electrode is suitable for the determination of UA. Additionally, the spiked and non-spiked samples were analyzed utilizing the standard HPLC method. As tabulated in Table 3, a good consistency was observed between the

results obtained with the proposed method and those of the standard method, pointing out the validity of the results [37].

4. Conclusions

Micro porous CeO₂ can be prepared using the self-propagation high-temperature method. Porous CeO₂ is a promising candidate for modifying a carbon paste electrode for voltammetric determination of UA. Because of its high surface area and good electrical conductivity, porous CeO₂ shows electrocatalytic activity towards the electro-oxidation of UA. In conclusion, CPE/porous CeO₂ exhibits great potential as an electrocatalyst for sensing trace amounts of UA in real samples with satisfactory results. Moreover, modified electrodes with micro porous CeO₂ can be tested for electrochemical detection of other pharmaceuticals in blood serum and urine samples and for monitoring the concentration of electroactive pollutants in waste water and river water samples.

Declaration of interests

The authors declare that they have no known competing financial interests or personal relationships that could have appeared to influence the work reported in this paper.

Table 3. Electrochemical determination of UA in diluted urine and serum samples with the proposed modified electrode and standard HPLC method ($n = 3$).

Sample	Proposed method			Standard method	
	Spiked (μM)	Found* (μM)	Recovery (%)	Found* (μM)	Recovery (%)
Urine	0.0	8.2±0.3	-	8.4±0.4	-
	5.0	12.9±0.5	97.7	13.3±0.6	99.2
	50.0	59.1±1.3	101.5	59.2±1.5	101.4
Serum	0.0	2.5±0.1	-	2.4±0.1	-
	5.0	7.2±0.3	96	7.6±0.3	102.7
	50.0	53.1±1.5	101.1	52.1±1.8	99.4

*Mean ± standard deviation.

References

- [1] Y.V. Manohara Reddy, Ba. Sravani, S. Agarwal, V.K. Gupta, G.Madhavi, Electrochemical sensor for detection of uric acid in the presence of ascorbic acid and dopamine using the poly (DPA)/SiO₂@Fe₃O₄ modified carbon paste electrode, *J. Electroanal. Chem.* 820 (2018) 168-175.
- [2] X. Gao, R. Gui, K. Qizhou Xu, H. Guo, H. Jin, Z. Wang, A bimetallic nanoparticle/graphene oxide/thionine composite-modified glassy carbon electrode used as a facile ratiometric electrochemical sensor for sensitive uric acid determination, *New J. Chem.* 42 (2018) 14796-14804.
- [3] T. Zhang, X. Sun, B. Liu, Synthesis of positively charged CdTe quantum dots and detection for uric acid, *Spectrochim. Acta A*, 79 (2011) 1566-1572.
- [4] X.-L. Li, G. Li, Y.-Z. Jiang, D. Kang, C.H. Jin, Q. Shi *et al.*, Human nails metabolite analysis: A rapid and simple method for quantification of uric acid in human fingernail by high-performance liquid chromatography with UV-detection, *J. Chromatogr. B*, 1002 (2015) 394-398.
- [5] L.I. Liu, L. Liu, Y. Wang, B.-C. Ye, A novel electrochemical sensor based on bimetallic metal-organic framework-derived porous carbon for detection of uric acid, *Talanta*, 199 (2019) 478-484.
- [6] S. Immanuel, T. Aparna, R. Sivasubramanian, A facile preparation of Au-SiO₂ nanocomposite for simultaneous electrochemical detection of dopamine and uric acid, *Surf. Interf.* 14 (2019) 82-91.
- [7] R. Sha, N. Vishnu, S. Badhulika, MoS₂ based ultra-low-cost, flexible, non-enzymatic and non-invasive electrochemical sensor for highly selective detection of uric acid in human urine samples, *Sensor. Actuat. B-Chem.* 279 (2019) 53-60.
- [8] C. Ma, P. Li, L. Xia, F. Qu, R.-M. Kong, Z.-L. Song, A novel ratiometric fluorescence nanoprobe for sensitive determination of uric acid based on CD@ZIF-CuNC nanocomposites, *Microchim. Acta*, 188 (2021) 1-10.
- [9] X. Qin, C. Yuan, G. Geng, R. Shi, S. Cheng, Y. Wang, Enzyme-free colorimetric determination of uric acid based on inhibition of gold nanorods etching, *Sensor. Actuat. B-Chem.* 333 (2021) 129638.
- [10] D. Cao, Y.-X. Luo, W.-P. Liu, Y.-S. Li, X.-F. Gao, Enzyme-free fluorescence determination of uric acid and trace Hg (II) in serum using Si/N doped carbon dots, *Spectrochim. Acta A*, 263 (2021) 120182.
- [11] Z. Chai, C. Zhang, H. Wang, X. Bi, P. Bai, X. Wang, Increased interface effects of PtFe alloy/CeO₂/C with PtFe selective loading on CeO₂ for superior performance in direct methanol fuel cell, *Int. J. Hydrogen Energ.* 44 (2019) 4794-4808.
- [12] A. Sengupta, M. Murali, P. Mohapatra, Electrochemical behavior of cerium (IV) in a RTIL and its mixture with ethanol, *J. Rare Earth.* 32 (2014) 641-647.
- [13] E.K. Goharshadi, S. Samiee, P. Nancarrow, Fabrication of cerium oxide nanoparticles: characterization and optical properties, *J. Colloid Interf. Sci.* 356 (2011) 473-480.
- [14] S. Xue, Q. Li, L. Wang, W. You, J. Zhang, R. Che, Copper- and cobalt-codoped CeO₂ nanospheres with abundant oxygen vacancies as highly efficient electrocatalysts for dual-mode electrochemical sensing of MicroRNA, *Anal. Chem.* 91 (2019) 2659-2666.
- [15] R. Murugan, G. Ravi, G. Vijayaprasath, S. Rajendran, M. Thaiyan, M. Nallappan *et al.*, Ni-CeO₂ Spherical nanostructures for magnetic and electrochemical supercapacitor applications, *Phys. Chem. Chem. Phys.* 19 (2017) 4396-4404.
- [16] Y. Hernández-Castillo, M. García-Hernández, A. López-Marure, J.H. Luna-Domínguez, P.Y. López-Camacho, Á. de J. Morales-Ramírez, Antioxidant activity of cerium oxide as a function of europium doped content, *Ceram. Int.* 45 (2019) 2303-2308.
- [17] Y.B. Choi, J.H. Son, D.S. Bae, Fabrication and characterization of Cu doped CeO₂ by hydrothermal process for antimicrobial activity, *Defect Diffus. Forum*, 391 (2019) 114-119.
- [18] X. Chen, G. Li, Y. Su, X. Qiu, L. Li, Z. Zou, Synthesis and room-temperature ferromagnetism of CeO₂ nanocrystals with nonmagnetic Ca²⁺ doping, *Nanotechnology*, 20 (2009) 115606.
- [19] G. Gottstein, *Physical Foundations of Materials Science*, Springer Science & Business Media, NY, 2013.
- [20] J.G. Omran, M.S. Afarani, M. Sharifitabar, Fast synthesis of MgAl₂O₄-W and MgAl₂O₄-W-W₂B composite powders by self-propagating high-temperature synthesis reactions, *Ceram. Int.* 44 (2018) 6508-6513.
- [21] A.A. Ensafi, R. Noroozi, N. Zandi-Atashbar, B. Rezaei, Cerium (IV) oxide decorated on

- reduced graphene oxide, a selective and sensitive electrochemical sensor for fenitrothion determination, *Sensor. Actuat. B-Chem.* 245 (2017) 980-987.
- [22] Z. Hashemzaei, M. Sharifitabar, H. Saravani, M. Noroozifar, Synthesis of porous Mg-doped CeO₂ powders via self-propagating high-temperature synthesis route, *Adv. Powder Technol.* 30 (2019) 2947-2956.
- [23] N. Bibi, Y. Xia, S. Ahmed, Y. Zhu, S. Zhang, A. Iqbal, Highly stable mesoporous CeO₂/CeS₂ nanocomposite as electrode material with improved supercapacitor electrochemical performance, *Ceram. Int.* 44 (2018) 22262-22270.
- [24] M. Shahbakhsh, S. Narouie, M. Noroozifar, Modified glassy carbon electrode with Polydopamine-multiwalled carbon nanotubes for simultaneous electrochemical determination of biocompounds in biological fluids, *J. Pharmaceut. Biomed.* 161 (2018) 66-72.
- [25] S.H. DuVall, R.L. McCreery, Control of catechol and hydroquinone electron-transfer kinetics on native and modified glassy carbon electrodes, *Anal. Chem.* 71 (1999) 4594-4602.
- [26] Y. Yue, G. Hu, M. Zheng, Y. Guo, J. Cao, S. Shao, A mesoporous carbon nanofiber-modified pyrolytic graphite electrode used for the simultaneous determination of dopamine, uric acid, and ascorbic acid, *Carbon*, 50 (2012) 107-114.
- [27] M. Shahbakhsh, M. Noroozifar, 2D-Single-crystal hexagonal gold nanosheets for ultra-trace voltammetric determination of captopril, *Microchim. Acta*, 186 (2019) 195.
- [28] M.I. Shekh, J. Amirian, B. Du, A. Kumar, G. Sharma, F.J. Stadler, J. Song, Electrospun ferric ceria nanofibers blended with MWCNTs for high-performance electrochemical detection of uric acid, *Ceram. Int.* 46 (2020) 9050-9064.
- [29] D. Li, M. Liu, Y. Zhan, Q. Su, Y. Zhang, D. Zhang, Electrodeposited poly (3,4-ethylenedioxythiophene) doped with graphene oxide for the simultaneous voltammetric determination of ascorbic acid, dopamine and uric acid, *Microchim. Acta*, 187 (2020) 1-10.
- [30] Q. Wang, H. Sun, Q. Liu, L. Li, J. Kong, Electrodeposition of three-dimensional network nanostructure PEDOT/PANI for simultaneous voltammetric detection of ascorbic acid, dopamine and uric acid, *ChemistrySelect*, 5 (2020) 1288-1293.
- [31] H. Karimi-Maleh, O.A. Arotiba, Simultaneous determination of cholesterol, ascorbic acid and uric acid as three essential biological compounds at a carbon paste electrode modified with copper oxide decorated reduced graphene oxide nanocomposite and ionic liquid, *J. Colloid Interf. Sci.* 560 (2020) 208-212.
- [32] Q. Wang, H. Si, L. Zhang, L. Li, X. Wang, S. Wang, A fast and facile electrochemical method for the simultaneous detection of epinephrine, uric acid and folic acid based on ZrO₂/ZnO nanocomposites as sensing material, *Anal. Chim. Acta*, 1104 (2020) 69-77.
- [33] M. Rees, A.G. Wright, S. Holdcroft P. Bertoncello, Voltammetry at hexamethyl-P-terphenyl poly (benzimidazolium)(HMT-PMBI)-coated glassy carbon electrodes: Charge transport properties and detection of uric and ascorbic Acid, *Sensors-Basel*, 20 (2020) 443.
- [34] K. Ghanbari, F. Nejabati, Ternary nanocomposite-based reduced graphene oxide/chitosan/Cr₂O₃ for the simultaneous determination of dopamine, uric acid, xanthine, and hypoxanthine in fish meat, *Anal. Methods-UK*, 12 (2020) 1650-1661.
- [35] W. Yao, H. Guo, H. Liu, Q. Li, N. Wu, L. Li, *et al.*, Highly electrochemical performance of Ni-ZIF-8/N S-CNTs/CS composite for simultaneous determination of dopamine, uric acid and L-tryptophan, *Microchem. J.* 152 (2020) 104357.
- [36] B. Demirkan, S. Bozkurt, K. Cellat, K. Arıkan, M. Yılmaz, A. Şavk *et al.*, Palladium supported on polypyrrole/reduced graphene oxide nanoparticles for simultaneous biosensing application of ascorbic acid, dopamine, and uric acid, *Sci. Rep.-UK*, 10 (2020) 2946.
- [37] M. Motshakeri, A.R. Phillips, P.A. Kilmartin, Application of cyclic voltammetry to analyse uric acid and reducing agents in commercial milks, *Food Chem.* 293 (2019) 23-31.